

Analysis of system dynamic influences in robotic actuators with variable stiffness

Philipp Beckerle^{*1}, Janis Wojtuscz^{2a},
Stephan Rinderknecht^{1b} and Oskar von Stryk^{2c}

¹*Institute for Mechatronic Systems in Mechanical Engineering, Technische Universität Darmstadt,
Petersenstraße 30, 64287 Darmstadt, Germany*

²*Simulation, Systems Optimization and Robotics Group, Technische Universität Darmstadt,
Hochschulstraße 10, 64289 Darmstadt, Germany*

(Received April 30, 2013, Revised November 20, 2013, Accepted December 14, 2013)

Abstract. In this paper the system dynamic influences in actuators with variable stiffness as contemporary used in robotics for safety and efficiency reasons are investigated. Therefore, different configurations of serial and parallel elasticities are modeled by dynamic equations and linearized transfer functions. The latter ones are used to identify the characteristic behavior of the different systems and to study the effect of the different elasticities. As such actuation concepts are often used to reach energy-efficient operation, a power consumption analysis of the configurations is performed. From the comparison of this with the system dynamics, strategies to select and control stiffness are derived. Those are based on matching the natural frequencies or antiresonance modes of the actuation system to the frequency of the trajectory. Results show that exclusive serial and parallel elasticity can minimize power consumption when tuning the system to the natural frequencies. Antiresonance modes are an additional possibility for stiffness control in the series elastic setup. Configurations combining both types of elasticities do not provide further advantages regarding power reduction but an input parallel elasticity might enable for more versatile stiffness selection. Yet, design and control effort increase in such solutions. Topologies incorporating output parallel elasticity showed not to be beneficial in the chosen example but might do so in specific applications.

Keywords: variable stiffness; series elastic actuation; parallel elastic actuation; elastic joints; dimensioning; control; robotics; system dynamics

1. Introduction

In conventional robotic applications, a precise, fast, and repetitive positioning of end effectors or manipulators is the most common task. This requires a robotic system with low compliance, accurate position control, and high joint torques. Therefore, general conventional robots are constructed of rigid links as well as joint actuators with high output power and high stiffness and

*Corresponding author, Dipl.-Ing., E-mail: beckerle@ims.tu-darmstadt.de

^a Dipl.-Ing., E-mail: wojtusch@sim.tu-darmstadt.de

^b Institute chair professor, E-mail: rinderknecht@ims.tu-darmstadt.de

^c Institute chair professor, E-mail: stryk@sim.tu-darmstadt.de

typically work in restricted areas to prevent any harmful interaction with humans. Due to an increasing demand in closer human-robot interaction - e.g., with domestic assistant robots or active prosthetic devices - there is a need for variable elastic joint actuation concepts that decouple actuator and joint and modify the stiffness dependent on the actual operating condition (van Ham *et al.* 2009, Lens and von Stryk 2012).

High stiffness is beneficial for enhanced precision, repeatability, and speed, while high compliance increases safety and energy absorption. The energy efficiency of oscillating movements can be enhanced by matching the natural frequency of an elastic actuator to the frequency of the desired trajectory as in Pratt and Williamson (1995), Vanderborght *et al.* (2009). An elastic actuator concept further allows protecting the mechanical setup by absorbing destructive shock loads and smoothing the robot motion.

In the middle of the 1990s, first actuator concepts with variable stiffness like the Series Elastic Actuator (SEA) by Pratt and Williamson (1995) and the Mechanical Impedance Adjuster (MIA) by Morita and Sugano (1995) have been introduced. While the force-controlled SEA is based on a fixed-stiffness spring in series with a stiff actuator, MIA adjusts the stiffness by changing the active length of a leaf spring. Starting from these actuator concepts, a large number of variable elastic actuators with various principles of adjusting the stiffness were presented in the following decades. In 2009, van Ham *et al.* (2009) categorized the fundamental principles into four groups: equilibrium controlled, structure controlled, mechanically controlled, and antagonistic controlled stiffness. While the equilibrium controlled principle changes the equilibrium position of a spring to generate a desired force or stiffness as in Hollander *et al.* (2005), the antagonistic controlled principle is based on two or more actuators with non-adaptable stiffness, coupled antagonistically and working against each other similar to human muscles (van Ham *et al.* 2009). Structure controlled elastic actuators change the stiffness due to a modification of the physical structure of an elastic element - e.g., the moment of inertia or the effective elastic length (van Ham *et al.* 2009). Mechanically controlled elastic actuators use the full length of the elastic element, but adjust the stiffness by modifying the pretension or preload as explained in van Ham *et al.* (2009). Most of the present actuator concepts can be sorted into these categories. The concepts of SEA, VS-Joint by Wolf and Hirzinger (2008), the iCub SEA module from Tsagarakis *et al.* (2009), and CompAct by Laffranchi *et al.* (2011) belong to the group of the equilibrium controlled stiffness, while the concepts of MIA, Jack Spring from Hollander *et al.* (2005), VSJ in Choi *et al.* (2011), and VTS by Schuy *et al.* (2012) represent structure controlled approaches. Examples for mechanically controlled concepts are MARIONET from Sulzer *et al.* (2005), MACCEPA in Vanderborght *et al.* (2009), Tunable Spring by Umedachi and Ishiguro (2006), V2E2 from Stramigioli *et al.* (2008), rHEA in Stienen *et al.* (2008), HDAU (Kim and Song 2010, Song and Kim 2010), vsaUT (Rao *et al.* 2011, Groothuis *et al.* 2012), AwAS (Jafari *et al.* 2010, Jafari *et al.* 2011), and MESTRAN from Quy *et al.* (2011). The PPAM concept is usually implemented in antagonistic setups as in Verrelst *et al.* (2000) and hence classified to the antagonistic controlled principle. Further concepts for antagonistic controlled stiffness are AMASC from Hurst *et al.* (2004), ANELS (Koganezawa *et al.* 2004), GATECH-SEA by Migliore *et al.* (2005), VSA (Tonietti *et al.* 2005, Schiavi *et al.* 2008), VSSEA from Thorson *et al.* (2007), PDAU (Song and Kim 2010), and Edinburgh-SEA by Mitrovic *et al.* (2010). The quasi-antagonistic approach QA-Joint in Eiberger *et al.* (2010) applies a serial elastic main actuator with modifying the stiffness by an additional antagonistic actuator. Beyond this categorization, there are concepts like SDAU (Song and Kim 2010) with a direct drive in combination with a deceleration actuator. Table 1 gives an overview on the given examples for existing variable elastic actuator concepts sorted by category in historical order.

Table 1 Overview on actuation concepts with variable elasticity

Equilibrium controlled	Structure controlled	Mechanically controlled	Antagonistic controlled
SEA (1995)	MIA (1995)	MARIONET (2005)	PPAM (2000)
VS-Joint (2008)	Jack Spring (2005)	MACCEPA (2006/09)	AMASC (2004)
iCub SEA (2009)	VSJ (2009)	Tun. Spring (2006)	ANELS (2004)
CompAct (2011)	VTS (2012)	V2E2 (2008)	GATECH-SEA (2005)
		rHEA (2008)	VSA (2005/08)
		HDAU (2010)	VSSEA (2007)
		vsUT (2010/11/12)	PDAU (2010)
		AwAS (2010/11)	QA-Joint (2010)
		MESTRAN (2011)	Edinburgh-SEA (2010)

Besides the underlying operation principle, the configuration and arrangement of elastic elements have a significant influence on the dynamic and energetic properties of an elastic actuator concept. Most present concepts with variable stiffness apply a serial elastic element to increase energy efficiency and safety in human-robot interaction. But likewise, the application of parallel elastic elements or combinations of serial and parallel elastic elements can be used to further reduce total energy and peak power requirements as in Mettin *et al.* (2009) or Grimmer *et al.* (2012).

In 2009, Mettin *et al.* (2009) studied the influence of parallel elastic elements on the driving of an underactuated planar two-link pendulum. The total energy consumption of the system could significantly be reduced by applying a tuned parallel spring mechanism to the actuated joint. In 2012, Grimmer *et al.* (2012) ran a simulation study on the peak power and total energy requirements of exclusive serial elastic, exclusive parallel elastic, and combined serial and parallel elastic actuators in a system mimicking human ankle joint motions. All configurations of elastic actuators with appropriate parameters were able to decrease peak power and total energy in comparison to a direct drive. An exclusive serial elastic configuration could reduce total energy consumption more than a parallel configuration, while an exclusive parallel elastic configuration was able to decrease peak power requirements more than a serial configuration. The combined configuration with serial and parallel elastic elements could lower the required peak power, but had less advantage in total energy consumption than an exclusive serial elastic actuator. Further, Eslamy *et al.* (2012) extended this investigation regarding unidirectional springs and Eslamy *et al.* (2013) considered the addition of damping. The results show that a parallel elasticity acting only unidirectional decreases energy requirements compared to the bidirectional solution and that introducing damping can be beneficial in descending stairs. These results suggest that dynamic and energetic properties of variable elastic actuator concepts can be optimized by choosing an appropriate combination of serial and parallel elements according to the given application.

Regarding the design of elastic actuators with variable stiffness, the dynamic characteristics of the system like inertia or gravitational effects have significant impact as shown in Beckerle *et al.* (2013a). Anyhow, design is focused on the drive properties considering the input inertia of the drive train only in early solutions like in Pratt and Williamson (1995). Although models including drive and link side properties of the drive train in the complete robotic application are used, those are mainly used for simulation as in Morita and Sugano (1997), but the dynamic interaction of input and output inertia is not sufficiently considered for dimensioning mostly. Since those early

concepts, energy efficiency due to energy storage in the compliant element became an additional requirement in the application of elastic actuation (van Ham *et al.* 2009). Due to this, the output inertia is focused but input inertia is not considered appropriately in the dimensioning of recent approaches, as the majority of those assume the drives to be ideal torque or position generators - e.g., in Jafari *et al.* (2011), Hollander *et al.* (2005), Sulzer *et al.* (2005) and Wolf and Hirzinger (2008). These assumptions are also used in Vanderborght *et al.* (2009) for a very insightful comparison of the power consumption of various concepts. Yet, without considering the inertia interaction during dynamic operation, it does not show the complete characteristics of those systems. Until now, the influence of more than a single inertia is especially considered in complex antagonistically-controlled concepts as AMASC from Hurst *et al.* (2004) and VSA by Tonietti *et al.* (2005). Among those the influence of interaction does not show significant influence on the characteristics of AMASC, while its impact is not examined in the case of VSA. In the structure-controlled and comparable complex VSJ from Choi *et al.* (2011), the interaction influence is rather low as in AMASC. In Beckerle *et al.* (2013a) the impact of fundamental system dynamic influences like input and output inertia as well as gravitation are investigated and described for a linearized model of a generic actuator with variable stiffness based on the parameters of VTS in Schuy *et al.* (2012). Further, Beckerle *et al.* (2013b) shows that considering those influences leads to more versatile possibilities in selecting stiffness in an analysis of power consumption compared to Vanderborght *et al.* (2009). These possibilities are due to the system dynamics showing two natural frequencies and an antiresonance. As stiffness can be selected fitting the antiresonance or second natural mode to the frequency of the trajectory, a wider range of operation can be covered.

This paper gives further insight to system dynamic influences on the design and control of actuators with variable stiffness based on (Beckerle *et al.* 2013a, b). Therefore, investigations are extended systematically to cover a wide range of drive train configurations and additional characteristics. In Section 2, the methods and models used to analyze the influences are presented. Beyond series elastic actuation as in (Beckerle *et al.* 2013a, b), different drive train configurations as parallel elastic actuation as well as the combinations of serial and parallel elements are considered. Further, the methods for power analysis and the investigation of stiffness variation are given. In Section 3, the results of the examinations on generic variable stiffness actuators with the different topologies with those methods are shown. Here, the impact on the transfer behavior and power consumption is presented and the influence of stiffness variation is given. Additionally, the significance of the different influences regarding the specific application is examined. Subsequently, a detailed discussion of the results and their relevance for design and control are given in Section 4. Finally, the paper and the main insights are concluded in Section 5.

2. Methods

In this section, the different configurations are described and the methods used for their investigation are presented. Based on the equations of motion modeling the nonlinear dynamics, linearized transfer functions and the corresponding eigenvectors are determined for system dynamic analysis. As their investigation focuses on the decomposition of dynamic effects, the impact of stiffness variation is not considered in this. Subsequently, the equations for inverse dynamics simulation of the investigated systems are presented for power analysis including stiffness variation. Finally, the characteristic frequencies are calculated for varying stiffness to examine their impact on natural behavior and control strategy.

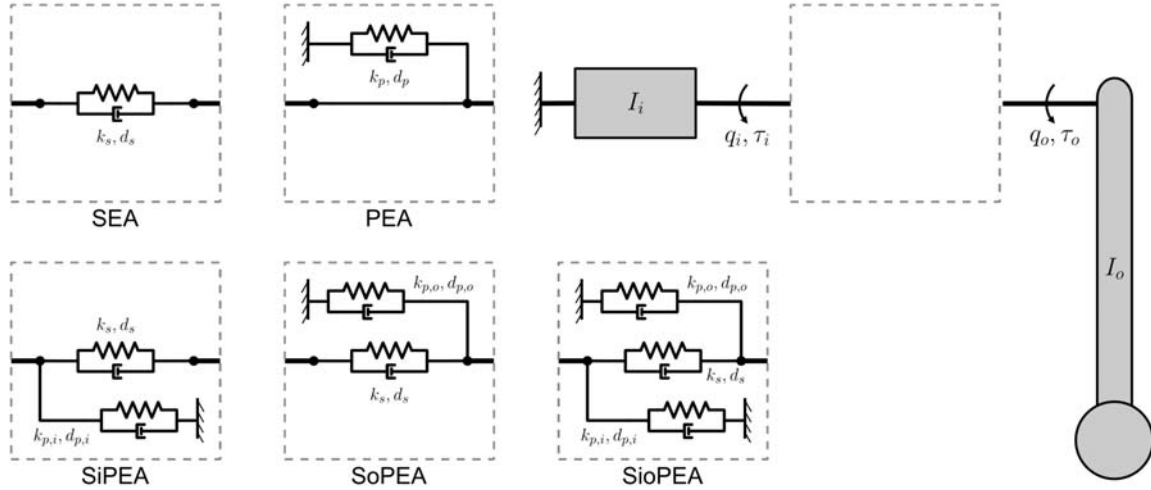


Fig. 1 Investigated actuator configurations with rotatory serial and parallel spring-damper units

2.1 Modeling

Investigations of the elastic actuator concepts are based on a simulation of a single degree of freedom pendulum motion with amplitude of 10° and a frequency ranging from 0.1 Hz to 3.5 Hz. The applied pendulum is modeled in reference to the limbs of the biped robot named Lucy (Vanderborcht *et al.* 2008) and the VTS prototype shown in Beckerle *et al.* (2013b). All mechanical parameters of the pendulum are given in Table 2.

In Fig. 1, the mechanical structure of all investigated configurations are presented considering rotatory elasticities and dampers. The exclusive serial elastic (SEA) and exclusive parallel elastic (PEA) configurations use only one spring-damper unit. In the serial and output parallel (SoPEA) and the serial and input parallel elastic (SiPEA) two damped elasticities are included, while the serial, input and output parallel elastic concept (SiOPEA) applies three spring-damper units.

A general description of elastic joint robot dynamics as in Albu-Schäffer (2001) is given by

$$M(q_o) \begin{bmatrix} \ddot{q}_o \\ \ddot{q}_i \end{bmatrix} + C(q_o, \dot{q}_o) \begin{bmatrix} \dot{q}_o \\ \dot{q}_i \end{bmatrix} + D \begin{bmatrix} \dot{q}_o \\ \dot{q}_i \end{bmatrix} + K \begin{bmatrix} q_o \\ q_i \end{bmatrix} + G(q_o) = \begin{bmatrix} 0 \\ \tau_i \end{bmatrix} \quad (1)$$

In this, q_i and q_o represent the input and output position, while τ_i is the corresponding input torque introduced to the joint mechanism by the actuator. The system matrices $M(q_o)$, $C(q_o, \dot{q}_o)$ and $G(q_o)$ describe inertial, coriolis and gravitational effects as in rigid robotics with

$$M(q_o) = \begin{bmatrix} I_o & S(q_o) \\ S^T(q_o) & I_i \end{bmatrix}.$$

The rotor/input inertias I_i of the actuators are separated from the link/output inertias I_o by serial elasticities. The serial stiffness parameters k_s as well as the parallel stiffness parameters at

the input $k_{p,i}$ and the output $k_{p,o}$ are combined in the stiffness matrix K , while damping is modeled accordingly in the damping matrix D . Those matrices are given by

$$K = \begin{bmatrix} k_s + k_{p,o} & -k_s \\ -k_s & k_s + k_{p,i} \end{bmatrix} \text{ and } D = \begin{bmatrix} d_s + d_{p,o} & -d_s \\ -d_s & d_s + d_{p,i} \end{bmatrix}.$$

In the inertia matrix $M(q_o)$, the coupling matrix $S(q_o)$ describing the inertial couplings between the joints of multi-joint robots appears. In this study $S(q_o) = 0$, since a single joint is investigated to isolate the actuation behavior. Thus, system matrices are given by

$$M = \begin{bmatrix} I_o & 0 \\ 0 & I_i \end{bmatrix}, \quad C = \begin{bmatrix} 0 \\ 0 \end{bmatrix} \text{ and } G(q_o) = \begin{bmatrix} m_o g l \sin q_o \\ 0 \end{bmatrix},$$

where M does not depend on the output position q_o , and I_o , I_i , d_s , $d_{p,i}$, $d_{p,o}$, k_s , $k_{p,i}$, $k_{p,o}$ and $m_o g l \sin(q_o)$ are scalars. In the case of an exclusive parallel configuration, the parameters in Fig. 1 are referred as k_p and d_p . For the examination of the impact of stiffness variation, the stiffness values k_s , k_p , $k_{p,i}$ and $k_{p,o}$ are treated as variable parameters.

Table 2 Simulation Parameters

Parameter	Value	Unit
m_o	6.81	kg
g	9.81	m s ⁻²
l	0.35	m
I_o	0.93	kg m ²
I_i	1.15	kg m ²
k_s	10 – 750	Nm rad ⁻¹
k_p	10 – 750	Nm rad ⁻¹
$k_{p,i}$	10 – 750	Nm rad ⁻¹
$k_{p,o}$	10 – 750	Nm rad ⁻¹
d_s	0	Nm s rad ⁻¹
d_p	0	Nm s rad ⁻¹
$d_{p,i}$	0	Nm s rad ⁻¹
$d_{p,o}$	0	Nm s rad ⁻¹

For the deduction of the specific models of the examined configurations from Eq. (1), the corresponding stiffness values are inserted or stiffness is set to zero/infinity. In case of the SEA all parallel elasticities are set to zero while for the PEA the serial elasticity is set to infinity. In the

combinations of serial elasticity with certain parallel elements, the excluded parallel elasticities are set to zero. When considering only serial damping d_s , the equations of motion of the SEA are

$$\begin{aligned} I_o \ddot{q}_o + m_o g l \sin(q_o) + d_s (\dot{q}_o - \dot{q}_i) + k_s (q_o - q_i) &= 0 \\ I_i \ddot{q}_i - d_s (\dot{q}_o - \dot{q}_i) - k_s (q_o - q_i) &= \tau_i \end{aligned} \tag{2}$$

for example. In this, $I_o \ddot{q}_o + m_o g l \sin(q_o)$ can be interpreted as the output side torque τ_o , which would be required from a direct drive. As shown in (Beckerle *et al.* 2013a, b), this model allows for a more appropriate investigation of the dynamics of such actuation systems and the selection of serial stiffness, if this is variable. For the parallel elastic configuration with stiffness k_p , the dynamic equation of motion is found to be

$$(I_i + I_o) \ddot{q}_o + m_o g l \sin(q_o) + d_p \dot{q}_o + k_p q_o = \tau_i \tag{3}$$

In this case, only one degree of freedom is relevant, since the dynamics of drive and link side are coupled rigidly and the system thus represents a second order time-delay element.

2.2 System dynamics

For the investigation of the system dynamics, the equations of motion of the investigated configurations considering all elasticities but only serial damping are linearized regarding the equilibrium position of the pendulum at 0° . By transforming those linear equations of motion to frequency domain, the transfer functions of the specific models are obtained. In contrast to the models from Vanderborght *et al.* (2009) or Schuy *et al.* (2012), two transfer functions are found for the model of the serial elastic configuration (SEA) as well as all combinations of serial and parallel elasticity (SiPEA, SoPEA and SioPEA) due to considering the input inertia. The transfer function from the input torque τ_i to the output position q_o of those systems is given by

$$\frac{q_o(s)}{\tau_i(s)} = \frac{b_{o,1}s + b_{o,0}}{c_{o,4}s^4 + c_{o,3}s^3 + c_{o,2}s^2 + c_{o,1}s + c_{o,0}} \tag{4}$$

and the transfer function from the input torque τ_i to the input position q_i is

$$\frac{q_i(s)}{\tau_i(s)} = \frac{b_{i,2}s^2 + b_{i,1}s + b_{i,0}}{c_{o,4}s^4 + c_{o,3}s^3 + c_{o,2}s^2 + c_{o,1}s + c_{o,0}} \tag{5}$$

For both transfer functions, the system characteristics represented by the natural frequencies are identical and given by the poles of transfer functions Eqs. (4) and (5). As can be seen from the nominator of Eq. (5), an antiresonance mode is occurring in addition to the two natural frequencies of the system. For the different configurations of elasticities, only the parameters vary, while the structure remains for all concepts (SEA, SiPEA, SoPEA and SioPEA). As the parallel elastic setup represents mechanical systems with one degree of freedom, it can be modeled by a second order transfer function

$$\frac{q_o(s)}{\tau_i(s)} = \frac{1}{c_{o,2}s^2 + c_{o,1}s + c_{o,0}} \quad (6)$$

As a second order dynamic system, such systems show only one natural frequency and no antiresonance. Table 3 gives the symbolic values of the coefficients in all different configurations.

Table 3 Coefficients of transfer functions

	SEA	PEA	SoPEA	SiPEA	SioPEA
$b_{o,1}$	k_s	1	k_s	k_s	k_s
$b_{o,1}$	d_s	0	d_s	d_s	d_s
$b_{i,0}$	$k_s + m_o gl$	0	$k_s + k_{p,o} + m_o gl$	$k_s + m_o gl$	$k_s + k_{p,o} + m_o gl$
$b_{i,1}$	d_s	0	d_s	d_s	d_s
$b_{i,2}$	I_o	0	I_o	I_o	I_o
$c_{o,0}$	$k_s m_o gl$	$k_p m_o gl$	$(k_{p,o} + m_o gl)k_s$	$k_{p,i} m_o gl +$ $(k_{p,i} + m_o gl)k_s$	$k_{p,i}(k_{p,o} + m_o gl$ $+ k_s) + k_s(k_{p,o} + m_o gl)$
$c_{o,1}$	$d_s m_o gl$	d_s	$(k_{p,o} m_o gl)d_s$	$(k_{p,i} + m_o gl)d_s$	$(k_{p,i} + k_{p,o} + m_o gl)d_s$
$c_{o,2}$	$(I_i + I_o)k_s$ $+ I_i m_o gl$	$(I_i + I_o)$	$I_i(k_{p,o} + k_s$ $+ m_o gl) + I_o k_s$	$I_o(k_{p,i} + k_s) +$ $I_i(k_s + m_o gl)$	$I_i(k_{p,o} + k_s + m_o gl) +$ $I_o(k_{p,i} + k_s)$
$c_{o,3}$	$(I_i + I_o)d_s$	0	$(I_i + I_o)d_s$	$(I_i + I_o)d_s$	$(I_i + I_o)d_s$
$c_{o,4}$	$I_i I_o$	0	$I_i I_o$	$I_i I_o$	$I_i I_o$

By investigating the eigenvectors of the model, the relative motion of the inertias at the specific natural frequency can be figured out. For the one degree of freedom case, it is obvious that no relevant insight can be expected, as no relative motion is possible. For two degree of freedom systems, the eigenvectors u are given by the solution of the eigenvalue problem

$$\left(M_g^{-1} \left(K + I \frac{dG}{dq_o} \Big|_{q_o=0^\circ} \right) - \omega^2 I \right) u = 0, \quad (7)$$

where I is a matrix identity with the dimension of M_g or K_g respectively, $\frac{dG}{dq_o} \Big|_{q_o=0^\circ}$ is the linearization of of gravitational effects in $G(q_o)$ and ω represents the natural frequencies of the system (Craig and Kurdila 2011).

2.3 Power analysis

For the power analysis of the drive train, the powers required to perform the motion of input $P_{m,i} = \tau_i \dot{q}_i$ and output $P_{m,o} = \tau_o \dot{q}_o$ are investigated based on the models specified in Section 2.1 and neglecting damping. The results are obtained by an inverse dynamics simulation based on the equations from De Luca (2000). Those allow for a calculation of the drive side trajectories based on the ones from the output in robots with serial elastic actuation and can be written as

$$q_i = q_o + k_s^{-1} \tau_o, \quad \dot{q}_i = \dot{q}_o + k_s^{-1} \dot{\tau}_o, \quad \ddot{q}_i = \ddot{q}_o + k_s^{-1} \ddot{\tau}_o \quad (8)$$

In this, the link side torque τ_o is differentiated twice with respect to time corresponding to the fourth order dynamics of the system. The motion energies of input and output are given by

$$E_{m,i} = \int_{t_m} |P_{m,i}| dt \quad \text{and} \quad E_{m,o} = \int_{t_m} |P_{m,o}| dt \quad (9)$$

The average power consumption P_i , required from the actuator, results from the energy consumption $E_{m,i}$ for link motion divided by the elapsed time t_m of five periods. In all simulations a sinusoidal trajectory with a magnitude of 10° is considered. For comparison, the power consumption of the direct drive $P_{m,o}$ is derived from the simulation. Further, the initial energy of the different models is considered in all simulations, since this represents the actual operational state and is compatible with the assumptions in Vanderborght *et al.* (2009) and Schuy *et al.* (2012). In contrast to those, the investigated stiffness interval ranges from 10 Nm rad^{-1} up to 750 Nm rad^{-1} , while frequencies from 0.1 Hz to 3.5 Hz are considered to clarify the system dynamic influences of the exclusive serial and parallel elastic configurations. The resulting characteristic maps provide the assessment of power consumption against trajectory frequency and selected stiffness. For investigation of the topologies combining serial and parallel elastic elements, frequency is fixed to 2.5 Hz and all stiffness parameters are iterated. Thus, the characteristic maps for SoPEA and SiPEA represent power against the two considered stiffness values, while for the SioPEA a three-dimensional space is found to assess power over the three stiffness parameters.

2.4 Stiffness Variation

As the impact of stiffness variation is especially important for the optimization of power consumption, it is investigated in comparison with results of power analysis. Therefore, natural frequencies and antiresonance frequencies of the undamped SEA and PEA are calculated from the linearized transfer functions for varying stiffness parameters. Those frequencies are compared to the power consumption obtained from inverse dynamics simulations varying stiffness parameters. From this, the causes of areas with low and high power are traced to specific frequencies corresponding to the natural dynamics of the systems. Based on the resulting relations, adjustment laws for stiffness selection can be derived for SEA as proposed in Beckerle *et al.* (2013b) as well as for PEA. In cases combining serial and parallel elasticities, no equivalent comparison can be given due to the number of variable parameters. Hence, characteristic maps and spaces for varying all stiffness parameters and neglecting damping are investigated at specific single frequencies.

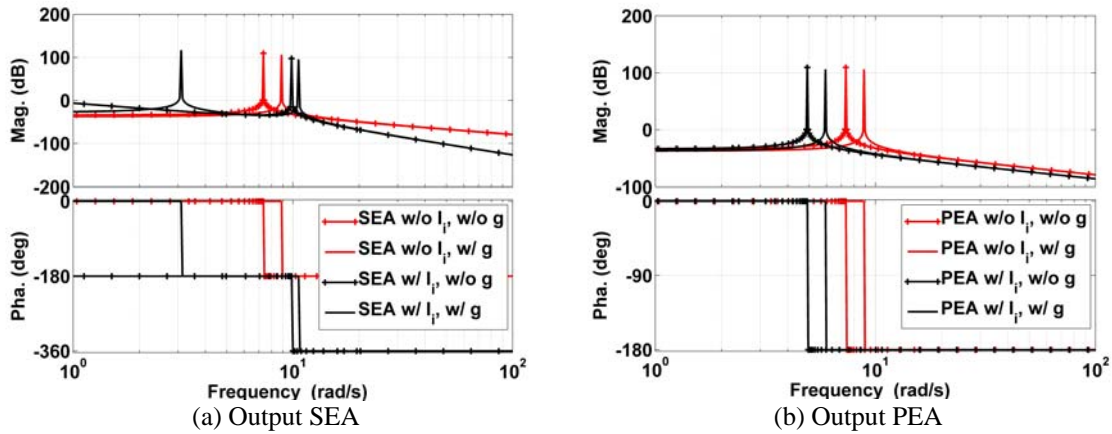


Fig. 2 Frequency response plots of configuration with one elasticity

3. Results

This section shows the results of the system dynamic investigation and shows the impact of input inertia and gravitation. Further, power analysis considering stiffness variation and the impact of stiffness variation on the natural behavior of the investigated example application are presented. As stiffness selection is a main issue in variable compliant actuators, adjustment laws to exploit natural dynamics are given.

3.1 System dynamics

By evaluating the linearized transfer functions from Section 2 with $k_s = 50 \text{ Nm rad}^{-1}$, $k_{p,i} = 50 \text{ Nm rad}^{-1}$ and $k_{p,o} = 50 \text{ Nm rad}^{-1}$ the system dynamics of the considered topologies and models are investigated. For serial elastic configuration a comparable investigation is given in Beckerle *et al.* (2013a). The transfer functions from the input torque τ_i to the output position q_o of SEA and PEA are shown in Figs. 2(a) and 2(b) for the serial and the parallel elastic configuration. In both, lines with plus signs indicate that gravitational effects are not considered, while those are included in results presented by solid lines. As gravitation is the only nonlinearity in the systems, transfer functions neglecting it are not linearized. The color of the lines depicts the investigated inertias: Results given in red do not contain the influence of input inertia I_i , while it is considered in results in black. Although input inertia is always physically present, it is not generally considered in modeling of elastic actuators. Hence, decomposition exposes deviations of the obtained models.

For the serial elastic configuration, it becomes distinct that gravity as well as input inertia increases the natural frequency as shown in Fig. 2(a). In case of gravity, this is due to the restoring torque $m_o g l \sin(q_o)$ that acts like a nonlinear spring and thus increases global system stiffness.

By introducing the input inertia I_i to the model while neglecting gravity, an additional rigid body mode occurs in the transfer behavior. This describes the rigid body motion of the two inertias for low frequencies and is characterized by global integral behavior showing a magnitude decrease of -40 dB/dec and a phase drop of 180° at 0 Hz. If the input inertia I_i and gravitational effects are considered, this rigid body mode is transformed to an elastic one. Due to this, the system has two elastic natural frequencies, as gravity has the effect of a virtual fixation of the link side. In case of the parallel elastic configuration, the influence of gravity is the same as in the serial elastic one as can be seen in Fig. 2(b). The natural frequency of the PEA system is increased due to the additional virtual stiffness introduced by the gravitational torque. In contrast to the serial elastic one, considering the input inertia introduces neither rigid body nor elastic modes, as the inertias of input and output are rigidly coupled. Hence, both inertias are observed as a single inertia I_i . Due to this higher inertia, only one elastic natural frequency showing a decreased value appears.

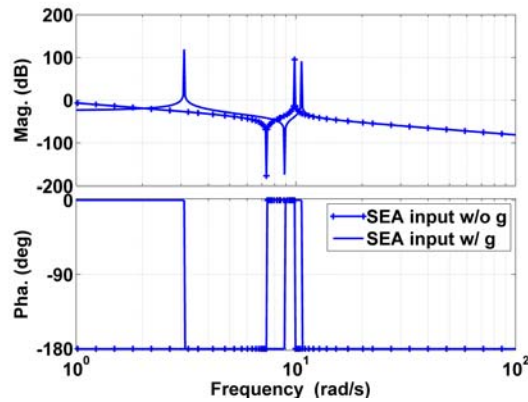


Fig. 3 Frequency response SEA input

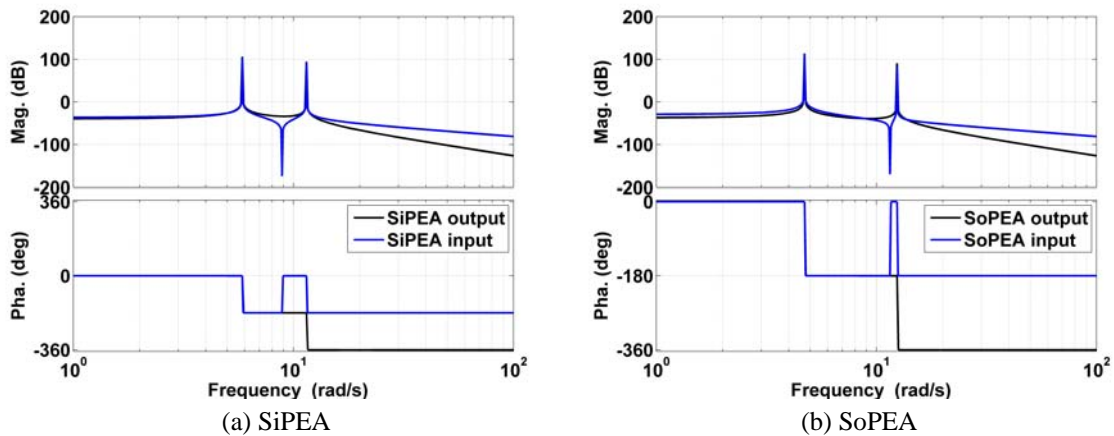


Fig. 4 Frequency response plots of configuration with two elasticities

Fig. 3 gives the transfer function from the input torque τ_i to the input position q_i for the serial elastic configuration. As this intrinsically requires considering both inertias, only the influence of gravity is examined. Besides the natural frequencies that also occur in the output transfer behavior, this transfer path shows an antiresonance mode due to the zero in the corresponding transfer function Eq. (5). When not considering gravity, global integral behavior due to the rigid body mode is observed as in the output transfer function. Introducing gravity leads to a virtual fixation due to the restoring torque $m_o g l \sin(q_o)$ that acts like a nonlinear spring and transforms the rigid body mode to an elastic one as in the output transfer function. In the parallel elastic drive train, this transfer function does not appear, since it has only one degree of freedom.

The transfer functions of the topologies combining serial and parallel elastic actuation are given in Figs. 4 and 5. In Fig. 4(a), the SiPEA configuration is shown, while the Fig. 4(b) plot depicts the combination of serial and output parallel elasticity. The black lines represent the transfer functions from the input torque τ_i to the output position q_o and the blue lines indicate the path from the input torque τ_i to the input position q_i . Both show comparable characteristics as the exclusive serial elastic system. Yet, the natural frequencies are compacted. In the case of the system with serial and input parallel elasticity, this effect is stronger than for the combination of serial and output parallel elasticity. Further, the natural and antiresonance modes in the SiPEA are distributed more equally than in the SoPEA or SEA.

Finally, the transfer behavior of the drive train containing all examined elasticities is given in Fig. 5. Here, the natural frequencies are further compacted compared to SiPEA. Anyhow, the distribution of the modes is not that even, since the antiresonance is very close to the second natural frequency.

Regarding the characteristic motion for operation in the elastic modes, the first eigenvector for all combinations (SEA, SiPEA, SoPEA and SioPEA) is $u_1 = [u_{11} \ 1]^T$. As u_{11} is always positive, both inertias move in phase and only the magnitude of the oscillation is altered due to the factor u_{11} . The second eigenvector of all those systems can be shown to be of the form $u_2 = [u_{21} \ 1]^T$, where u_{21} is always negative. During operation in this mode, the inertias are thus moving in antiphase and the output inertia is amplified by u_{21} .

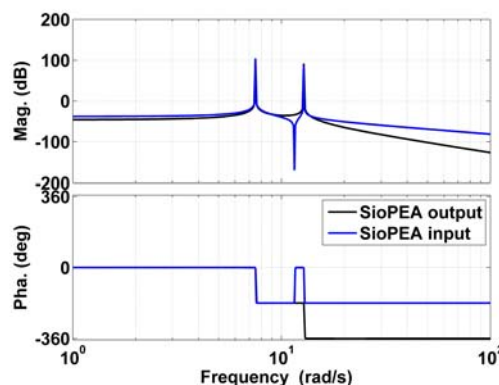


Fig. 5 Frequency response SioPEA

The influence of damping would be the same for all plots: If a positive definite and thus mechanically valid damping matrix is assumed, the resonance peaks of the elastic modes are decreased while the low points due to the antiresonance increase. A comparable effect could be observed in the phase response, which will be flattened as well, and the characteristic frequencies will be slightly shifted. Yet, including damping does not give further insight regarding principle design issues or power-optimized stiffness control, it is not further investigated here and the basic characteristics of the system dynamics are focused.

3.2 Power analysis

Subsequently, the power consumption of the different configurations calculated from the inverse dynamics simulation is presented. In all plots except the one for SioPEA, the power consumption of direct drive is given by black border for comparison.

In Fig. 6 the average power consumption of the SEA and PEA determined from inverse dynamics are plotted against the investigated frequencies and stiffness values as given in Section 2.3. For the SEA, three areas of minimal power consumption can be observed. The first one is caused by the first elastic mode of the system. Since this frequency is below 1.0 Hz and power consumption is generally low in this range, it is not relevant for stiffness variation to optimize power consumption. Beyond this, the antiresonance and the second natural frequency are leading to further areas of low power. As those cover the operating range when stiffness is varied, their utilization is suitable to reduce power consumption. This is possible by applying stiffness values below $k_s = 440 \text{ Nm rad}^{-1}$ and hence it is not necessary to exploit the whole investigated interval. The results for the parallel elastic setup are shown in Fig. 6(b). As it is obvious when considering the transfer function, only one area of minimal power consumption occurs that is due to the natural frequency of the system. Since this mode shows lower values compared to SEA due to the higher inertia, the low power area only covers frequencies up to 3.0 Hz. Therefore, stiffness reaches up to $k_p = 750 \text{ Nm rad}^{-1}$. Thus, the operating frequency range is not covered completely and the required stiffness interval is increased.

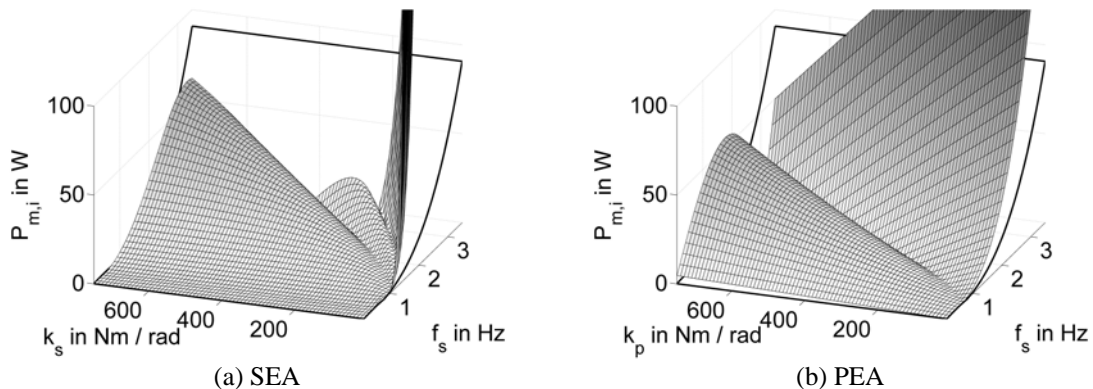


Fig. 6 Average power consumptions of configuration with one elasticity

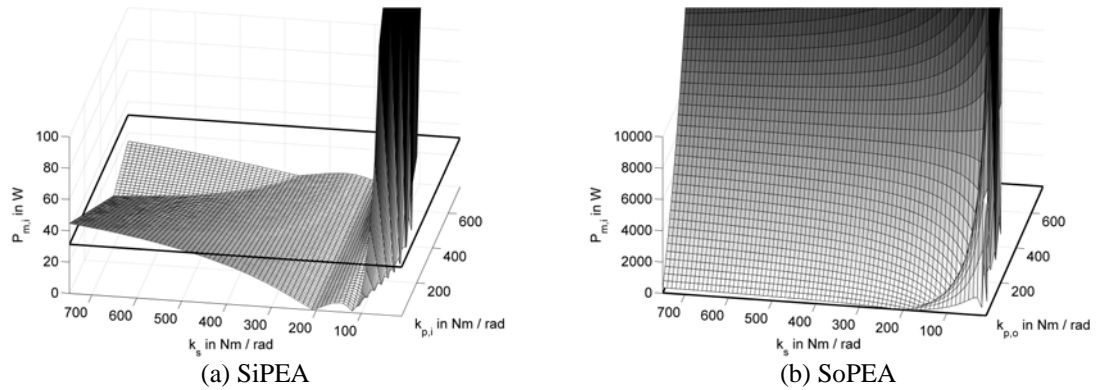


Fig. 7 Average power consumptions of configuration with two elasticities

The average power consumption of the SiPEA and the SoPEA are given in Figs. 7(a) and 7(b). As those depend on varying serial and a parallel stiffness, the powers are plotted against those at a fixed frequency of 2.5 Hz. When selecting low parallel stiffness, the minimum power areas for the SiPEA in Fig. 7(a) correspond to those of the SEA. Additionally, a new minimum area appears for certain combinations of higher serial and parallel stiffness values. Those provide comparable power requirements compared to the SEA but require more stiffness variation at higher values, which leads to higher control effort. In results for the SoPEA depicted in Fig. 7(b) one can clearly see that this configuration is not suitable, since the power consumption is unacceptably high. This negative effect rises with increasing output parallel stiffness values $k_{p,o}$.

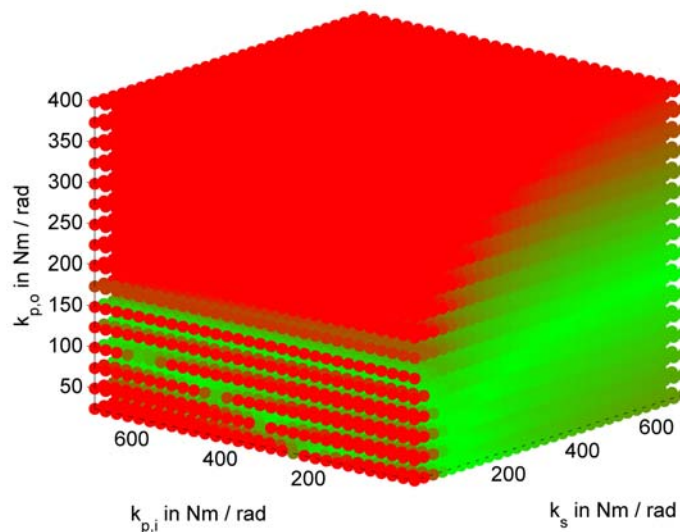


Fig. 8 Average power consumption of SioPEA

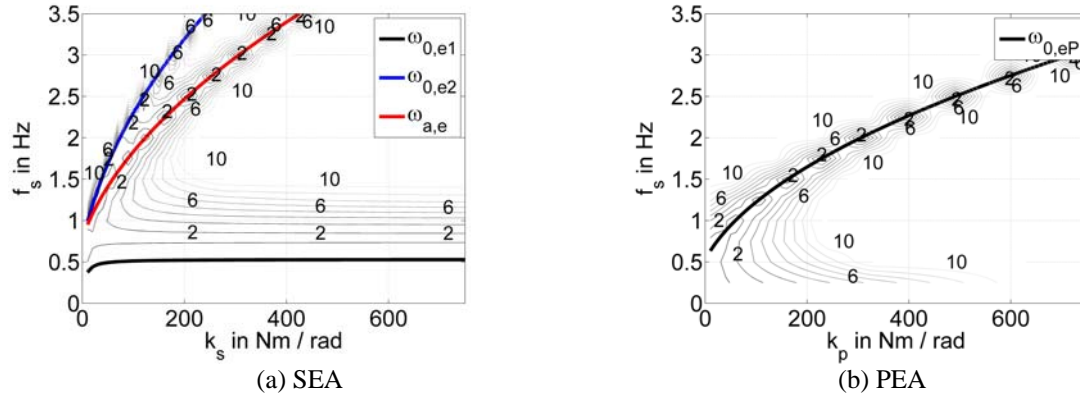


Fig. 9 Influence of stiffness variation in configurations with one elasticity

The scatter plot in Fig. 8 presents the average power consumption of the SioPEA with all elasticities. Power consumption is indicated by the mixture of green and red color of the points: A higher part of green represents lower consumption, while a higher share of red states higher consumption. Power consumptions of above 100 W are all depicted in exclusive red color, as those are assumed to be not feasible. As all investigated points with $k_{p,o} \geq 400 \text{ Nm rad}^{-1}$ exceed this value, those combinations are excluded from the plot. In analogy to SoPEA, output parallel stiffness $k_{p,o}$ shows negative effect on global power consumption. As for SEA and PEA, low power consumptions can be reached using k_s and $k_{p,i}$. Yet, the highest sensitivity for stiffness adjustment can be reached by using exclusive serial elasticity.

3.3 Stiffness variation

Investigating the influence of stiffness variation on system dynamics is crucial for the deduction of power-optimized stiffness selection strategies as shown in Beckerle *et al.* (2013b).

Figs. 9(a) and 9(b) depict the variation of the natural and antiresonance frequencies of the linearized models of SEA and PEA in comparison to the corresponding contour of the motion power consumption. As the modes show good concordance with the power minima from nonlinear inverse dynamics simulation, the approximation of the nonlinear dynamics by the natural behavior of the linearized models is appropriate. For the SEA shown in Fig. 9(a), the first natural frequency $\omega_{0,e1}$ at about 0.5 Hz is influenced by stiffness variation weakly (black line). Additionally, the level of power consumption in the surrounding of this area is rather low. In contrast to this, the second elastic mode $\omega_{02,e}$ can be manipulated better by stiffness adjustment and provides significant decrease of power consumption (blue line). Beyond those modes, the antiresonance $\omega_{a,e}$ due to the zero of Eq. (5) is observed (red line). The frequency of this mode only depends on the output characteristics. As the second elastic mode, the antiresonance can be manipulated well by stiffness adjustment and provides significant decrease of power consumption. Regarding the

impact of stiffness variation, the antiresonance as well as the second natural frequency are relatively sensitive and cover the whole investigated frequency range. Based on the relations between power minima and natural dynamics, model-based strategies for setting stiffness in series elastic configuration can be derived as

$$k_{s,a,e}(\omega) = I_o \omega^2 - m_o gl \quad (10)$$

for matching the antiresonance frequency $\omega_{a,e}$ and

$$k_{s,02,e}(\omega) = -\frac{I_i I_o \omega^4 - I_i m_o gl \omega^2}{-(I_o + I_i) \omega^2 + m_o gl} \quad (11)$$

for adjusting the system to the second natural frequency $\omega_{02,e}$ like it is shown for the example of serial elastic VTS in Beckerle *et al.* (2013b). Hence, power-optimized operation can be achieved by tuning k_s to the values $k_{s,a,e}(\omega)$ or $k_{s,02,e}(\omega)$. In Beckerle *et al.* (2013b), it is also suggested to tune the drive train based on either the second natural or the antiresonance frequency depending on the current application scenario to extend the operating range. As can be seen in Section 3.1 and Fig. 9(b), the parallel elastic configuration shows only one natural frequency $\omega_{0,eP}$. This is due to the coupling of the input and output inertia as $I_i + I_o$, which results in a decrease of the natural frequency and less sensitivity to stiffness variation. Thus, higher stiffness values have to be included to cover the investigated frequencies by the adjustment law

$$k_{p,e}(\omega) = (I_i + I_o) \omega^2 - m_o gl \quad (12)$$

This leads to an increased control activity for stiffness variation of $k_{p,e}(\omega)$ to match natural frequency $\omega_{0,eP}$ and thus should have negative impact on the efficiency of the whole actuation system. As a basis to develop strategies for stiffness variation for the SiPEA and the SoPEA, one can consider the power consumption plots of those for a trajectory with a frequency of 2.5 Hz in Fig. 7. In Fig. 7(a), the results for the SiPEA are shown. It becomes distinct that there are two possibilities to select the stiffness parameters: The first possibility is to tune serial stiffness to the modes of the SEA independently from the input parallel stiffness, as becomes obvious when comparing the power plots of SEA and SiPEA. The second parameter configuration is a more balanced combination of input parallel and serial stiffness and would thus require higher stiffness values. In Fig. 7(b) depicting the consumption of the SoPEA shows significantly increasing power consumption for increasing output stiffness. This indicates that the power-optimized selection of output parallel stiffness is zero and thus this concept is not beneficial compared to the SEA for this frequency. For the SioPEA the parameter selection is most complex, as the values for input parallel, output parallel and serial elasticity have to be chosen. Fig. 8 shows a scatter plot of the power consumptions for different configurations of those parameters. As for the SoPEA, one can see that the output parallel stiffness should be chosen to zero, since power requirements increase with this parameter (indicated by red color). Hence, it does not provide additional design freedoms compared to the SiPEA for this frequency.

4. Discussion

This study shows that investigating variable stiffness actuators with extended models including input and output dynamics, allows for more appropriate power-optimized stiffness selection regarding system dynamics. Anyhow, the influence of input dynamics depends on gear ratio and motor inertia given by the specific application. The example investigated here incorporates parameters from the VTS prototype of the authors as in Beckerle *et al.* (2013b). In this system, the reflected input and the output inertia are at similar levels and thus contribute equally.

Based on the frequency responses of the investigated configurations, the dynamic behavior can be understood and frequencies used for stiffness selection can be identified. Including input and output dynamics helps to clarify the characteristic actuator behavior. The comparison of the characteristic frequencies obtained from the linearized transfer functions with the results of power analysis shows that the latter ones are appropriate to represent the system dynamics in this example. For trajectories with higher amplitude, this might not be the case in general. As actuator configurations combining serial and parallel elasticities compact the characteristic frequencies of the system, those might allow for a better distribution of those over the range of operation. In this, the SiPEA shows to have the most balanced distribution.

Regarding power consumption, SEA and PEA decrease requirements compared to direct drive. SEA provides more possibilities to tune stiffness, as the antiresonance and second natural mode can be selected or even be combined. PEA requires higher stiffness bandwidth to cover the range of operation in comparison with SEA, which results in higher stiffness control effort and thus decreases global efficiency. In comparison to the SEA, the SiPEA introduces a new power minimal area. Although this might deliver new possibilities for stiffness control, the required control effort could cancel out the benefits, since higher stiffness values are required and serial as well as both serial and parallel stiffness have to be adjusted. As the output parallel stiffness in SoPEA leads to very high power consumption, this element might not to be applicable. This does not match the results from Grimmer *et al.* (2012) stating that this combination represents a trade-off between the advantages of SEA and PEA. Due to the application with a non-sinusoidal trajectory considered there, the reason for lower power consumption might be caused by the pretension of parallel stiffness that is not considered in this study. In analogy to the SoPEA, the SioPEA shows no improvements compared to SEA and PEA due to the negative influence of the parallel stiffness. An additional limitation of the configurations with multiple elasticities is the increased complexity affecting mechanical and control design. In contrast to this study, the results of power analysis in practical application could be altered by actuator efficiency and friction as those are not considered here.

For the selection of power-optimized stiffness, adjustment laws are derived from the linearized transfer functions. The lowest natural frequency of the SEA does not help to minimize power, as power consumption of the direct drive is comparable low at this frequency. In the investigated operating range, matching the antiresonance or second natural frequency to the trajectory allows to decrease power consumption distinctly. For the PEA, only one natural frequency occurs and higher stiffness values have to be included to cover the frequency range. Increased control effort resulting from this might affect power efficiency. In the configurations combining elasticities, there is no closed solution for stiffness control. Yet, the additional degrees of freedom extend the stiffness variation space, which might help to avoid areas with high power consumption. Appropriate parameter combinations might be found by optimization methods. Anyhow, the additional mechanical and control effort required to tune multiple elasticities has to be considered.

5. Conclusions

In this study, the system dynamic influences in actuators with variable elasticity are investigated and their relevance for design and control of those is presented. Results show that exclusive serial and parallel elasticity reduces power consumption by adjusting stiffness to match the characteristic frequency of the actuation system to the one of the trajectory. Adjustment laws for this purpose are derived from natural and antiresonance modes of linearized transfer functions of SEA and PEA. With those, stiffness variation can be conducted more versatile. As in the SEA a lower stiffness bandwidth compared to PEA is required, it should be beneficial for frequent stiffness variation due to the increased control effort that would appear in PEA. The combination of serial and input parallel elements can introduce additional degrees of freedom for stiffness selection but increases mechanical and control effort. Further, a closed solution for stiffness selection cannot be found. Anyhow, the adjustment laws of the SEA can be utilized to tune the SiPEA for low input elasticity. Due to this and the positive effect of the input parallel elasticity on the distribution of the modes, a fixed input parallel elasticity might be used in SiPEA configuration to modify the frequency range covered by the modes. In this case, adjustment can be performed modifying the SEA law to match SiPEA including this fixed stiffness. Utilization of output parallel elasticities shows to provide no advantages in general applications as comparable challenges arise for stiffness selection and power consumption is significantly increased. Other studies show that specific applications can profit from such configurations, if using pretension to customize the actuation system to the application.

Acknowledgments

The research described in this paper was financially supported by the Forum for Interdisciplinary Research of Technische Universität Darmstadt.

References

- Albu-Schäffer, A. (2001), *Regelung von Robotern mit elastischen Gelenken am Beispiel der DLR-Leichtbauarme*, Ph.D. Dissertation, Technische Universität München, Munich.
- Beckerle, P., Wojtusich, J., Rinderknecht, S. and von Stryk, O. (2013), "Mechanical influences on the design of actuators with variable stiffness", *Proceedings of the 6th International Symposium On Adaptive Motion Of Animals And Machines*, Darmstadt, March.
- Beckerle, P., Wojtusich, J., Schuy, J., Strah, B., Rinderknecht, S. and von Stryk, O. (2013), "Power-optimized stiffness and nonlinear position control of an actuator with variable torsion stiffness", *Proceedings of the IEEE/ASME International Conference on Advanced Intelligent Mechatronics*, Wollongong, July.
- Choi, J., Hong, S., Lee, W., Kang, S. and Kim, M. (2011), "A robot joint with variable stiffness using leaf springs", *IEEE T. Robot.*, **27**, 229-238.
- Craig, R.R. and Kurdila, A.J. (2011), *Fundamentals of structural dynamics*, John Wiley & Sons, Hoboken, New Jersey, United States.
- Eiberger, O., Haddadin, S., Weis, M., Albu-Schäffer, A. and Hirzinger, G. (2010), "On joint design with intrinsic variable compliance: derivation of the DLR QA-Joint", *Proceedings of the IEEE International Conference on Robotics and Automation*, Anchorage, May.
- Eslamy, M., Grimmer, M. and Seyfarth, A. (2012), "Effects of unidirectional parallel springs on required peak power and energy in powered prosthetic ankles: comparison between different active actuation concepts", *Proceedings of the IEEE International Conference on Robotics and Biomimetics*, Guangzhou, December.

- Eslamy, M., Grimmer, M., Rinderknecht, S. and Seyfarth, A. (2013), "Does it pay to have a damper in a powered ankle prosthesis? A Power-Energy Perspective", *Proceedings of the IEEE International Conference on Rehabilitation Robotics*, Seattle, June.
- Grimmer, M., Eslamy, M., Gliuch, S. and Seyfarth, A. (2012), "A comparison of parallel-and series elastic elements in an actuator for mimicking human ankle joint in walking and running", *Proceedings of the IEEE International Conference on Robotics and Automation*, St. Paul, May.
- Groothuis, S.S., Rusticelli, G., Zucchelli, A., Stramigioli, S. and Carloni, R. (2012), "The vsaUT-II: a novel rotational variable stiffness actuator", *Proceedings of the IEEE International Conference on Robotics and Automation*, St. Paul, May.
- Hollander, K.W., Sugar, T.G. and Herring, D.E. (2005), "Adjustable robotic tendon using a 'Jack Spring'", *Proceedings of the IEEE International Conference on Rehabilitation Robotics*, Chicago, June.
- Hurst, J.W., Chestnutt, J.E., and Rizzi, A.A. (2004), "An actuator with physically variable stiffness for highly dynamic legged locomotion", *Proceedings of the IEEE International Conference on Robotics and Automation*, New Orleans, April.
- Jafari, A., Tsagarakis, N.G. and Caldwell, D.G. (2011), "AwAS-II: A new Actuator with Adjustable Stiffness based on the novel principle of adaptable pivot point and variable lever ratio", *Proceedings of the IEEE International Conference on Robotics and Automation*, Shanghai, May.
- Jafari, A., Tsagarakis, N.G., Vanderborght, B. and Caldwell, D.G. (2010), "A novel actuator with adjustable stiffness (AwAS)", *Proceedings of the IEEE/RSJ International Conference on Intelligent Robots and Systems*, Taipei, October.
- Kim, B. and Song, J. (2010), "Hybrid dual actuator unit: A design of a variable stiffness actuator based on an adjustable moment arm mechanism", *Proceedings of the IEEE International Conference on Robotics and Automation*, Anchorage, May.
- Koganezawa, K., Shimizu, Y., Inomata, H. and Nakazawa, T. (2004), "Actuator with Non Linear Elastic System (ANLES) for controlling joint stiffness on antagonistic driving", *Proceedings of the IEEE International Conference on Robotics and Biomimetics*, Shenyang, August.
- Laffranchi, M., Tsagarakis, N. and Caldwell, D.G. (2011), "A compact compliant actuator (CompAct) with variable physical damping", *Proceedings of the IEEE International Conference on Robotics and Automation*, Shanghai, May.
- Lens, T. and von Stryk, O. (2012), "Investigation of safety in human-robot-interaction for a series elastic, tendon-driven robot arm", *Proceedings of the IEEE/RSJ International Conference on Intelligent Robots and Systems*, Vilamoura, October.
- De Luca, A. (2000), "Feedforward/feedback laws for the control of flexible robots", *Proceedings of the IEEE International Conference on Robotics and Automation*, San Francisco, April.
- Mettin, U., La Hera, P.X., Freidovich, L.B. and Shiriaev, A.S. (2009), "Parallel elastic actuators as a control tool for replanned trajectories of underactuated mechanical systems", *Int. J. Robot. Res.*, **29**(9), 1186-1198.
- Migliore, S.A., Brown, E.A., and DeWeerth, S.P. (2005), "Biologically inspired joint stiffness control", *Proceedings of the IEEE International Conference on Robotics and Automation*, Barcelona, April.
- Mitrovic, D., Klanke, S., Howard, M. and Vijayakumar, S. (2010), "Exploiting sensorimotor stochasticity for learning control of variable impedance actuators", *Proceedings of the IEEE-RAS International Conference on Humanoid Robots*, Nashville, December.
- Morita, T. and Sugano, S. (1995), "Design and development of a new robot joint using a mechanical impedance adjuster", *Proceedings of the IEEE International Conference on Robotics and Automation*, Nagoya, May.
- Morita, T. and Sugano, S. (1997), "Development and Evaluation of Seven-D.O.F. MIA ARM", *Proceedings of the IEEE International Conference on Robotics and Automation*, Albuquerque, May.
- Pratt, G.A. and Williamson, M.M. (1995), "Series elastic actuators", *Proceedings of the IEEE/RSJ International Conference on Intelligent Robots and Systems*, Pittsburgh, August.
- Quy, H.V., Aryananda, L., Sheikh, F.I., Casanova, F. and Pfeifer, R. (2011), "A novel mechanism for varying stiffness via changing transmission angle", *Proceedings of the IEEE International Conference on Robotics*

- and Automation, Shanghai, May.
- Rao, S., Carloni, R. and Stramigioli, S. (2011), "A novel energy-efficient rotational variable stiffness actuator", *Proceedings of the Annual International Conference of the IEEE Engineering in Medicine and Biology Society*, Boston, August.
- Schiavi, R., Grioli, G., Sen, S. and Bicchi, A. (2008), "VSA-II: a novel prototype of variable stiffness actuator for safe and performing robots interacting with humans", *Proceedings of the IEEE International Conference on Robotics and Automation*, Pasadena, May.
- Schuy, J., Beckerle, P., Wojtusich, J., Rinderknecht, S. and von Stryk, O. (2012), "Conception and evaluation of a novel variable torsion stiffness for biomechanical applications", *Proceedings of the IEEE International Conference on Biomedical Robotics and Biomechanics*, Roma, June.
- Song, J. and Kim, B. (2010), "Three types of dual actuator units for variable impedance actuation", *Proceedings of the IEEE International Conference on Robotics and Automation*, Anchorage, May.
- Stienen, A.H., Hekman, E.E., ter Braak, H., Aalsma, A.M., van der Helm, F.C. and van der Kooij, H. (2008), "Design of a rotational hydro-elastic actuator for an active upper-extremity rehabilitation exoskeleton", *Proceedings of the IEEE International Conference on Biomedical Robotics and Biomechanics*, Scottsdale, October.
- Stramigioli, S., van Oort, G. and Dertien, E. (2008), "A concept for a new energy efficient actuator", *Proceedings of the IEEE/ASME International Conference on Advanced Intelligent Mechatronics*, Xi'An, July.
- Sulzer, J.S., Peshkin, M.A. and Patton, J.L. (2005), "MARIONET: an exotendon-driven rotary series elastic actuator for exerting joint torque", *Proceedings of the IEEE International Conference on Rehabilitation Robotics*, Chicago, June.
- Thorson, I., Svinin, M. and Hosoe, S. (2007), "Design considerations for a variable stiffness actuator in a robot that walks and runs", *Proceedings of the Robotics and Mechatronics Conference*, Akita, May.
- Tonietti, G., Schiavi, R. and Bicchi, A. (2005), "Design and control of a variable stiffness actuator for safe and fast physical human/robot interaction", *Proceedings of the IEEE International Conference on Robotics and Automation*, Barcelona, April.
- Tsagarakis, N.G., Laffranchi, M., Vanderborght, B. and Caldwell, D.G. (2009), "A compact soft actuator unit for small scale human friendly robots", *Proceedings of the IEEE International Conference on Robotics and Automation*, Kobe, May.
- Umedachi, T. and Ishiguro, A. (2006), "A development of a fully self-contained real-time tunable spring", *Proceedings of the IEEE International Conference on Intelligent Robots and Systems*, Beijing, October.
- van Ham, R., Sugar, T. G., Vanderborght, B., Hollander, K. W. and Lefeber, D. (2009), "Compliant actuator designs review of actuators with passive adjustable compliance/controllable stiffness for robotic applications", *IEEE Robot. Autom. Mag.*, **16**(3), 81-94.
- Vanderborght, B., van Ham, R., Lefeber, D., Sugar, T.G. and Hollander, K.W. (2009), "Comparison of mechanical design and energy consumption of adaptable, passive-compliant actuators", *Int. J. Robot. Res.*, **28**, 90-103.
- Vanderborght, B., Tsagarakis, N.G., Semini, C., van Ham, R. and Caldwell, D.G. (2009), "MACCEPA 2.0: Adjustable compliant actuator with stiffening characteristic for energy efficient hopping", *Proceedings of the IEEE International Conference on Robotics and Automation*, Kobe, May.
- Vanderborght, B., Verrelst, B., van Ham, R., Damme, M., Beyl, P. and Lefeber, D. (2008), "Development of a compliance controller to reduce energy consumption for bipedal robots", *Auton. Robot.*, **24**(4), 419-434.
- Verrelst, B., Daerden, F., Lefeber, D., van Ham, R. and Fabri, T. (2000), "Introducing pleated pneumatic artificial muscles for the actuation of legged robots: a one-dimensional set-up", *Proceedings of the Climbing and Walking Robots*, Madrid, October.
- Wolf, S. and Hirzinger, G. (2008), "A new variable stiffness design: Matching requirements of the next robot generation", *Proceedings of the IEEE International Conference on Robotics and Automation*, Pasadena, May.